J dependences of the isotope shift and hyperfine structure in the Sm I $4f^6 5d\,6s\ ^9H$ term

W. G. Jin
Cyclotron Laboratory, The Institute of Physical and Chemical Research (RIKEN), Wako, Saitama 351-01, Japan

T. Horiguchi, W. Yang,* and I. Endo
Department of Physics, Faculty of Science, Hiroshima University, Higashi-Hiroshima 724, Japan
(Received 13 December 1993)

Isotope shifts and hyperfine structures of twelve transitions from the high-lying metastable ^9H_J ($J=1-7$) states of the $4f^6 5d\,6s$ configuration in Sm I have been measured for the stable isotopes by means of atomic-beam laser spectroscopy. Hyperfine constants A and B for the odd-mass isotopes ^{147}Sm and ^{149}Sm are determined for the ^9H_J ($J=1-7$) states and six upper levels of the transitions in Sm I. J dependences of the isotope shifts are observed for the $4f^6 5d\,6s\ ^9H$ term. Parameters z_{5d} of the crossed-second-order effect are derived for the $4f^6 5d\,6s$ configuration, and z_{5d}/λ is found to be 165(10) MHz/fm^2. It has been verified that the field shift is dominant in the crossed-second-order effect.

PACS number(s): 32.30.Jc, 32.70.Jz, 35.10.Fk

I. INTRODUCTION

Studies of isotope shift (IS) and hyperfine structure (hfs) for Sm stable isotopes have been of repeated interest to spectroscopists because there are great changes in the nuclear size on the one hand and many strong optical transitions suitable to IS and hfs measurements on the other hand. For the odd-mass isotopes ^{147}Sm and ^{149}Sm, the hfs constants A and B for the ground-state ^7F term of the $4f^6 6s^2$ configuration were precisely measured by means of the atomic-beam magnetic-resonance technique [1], and those of some high-lying excited levels were determined by means of laser spectroscopy [2,3]. Isotope shifts of several transitions from the low-lying metastable states of the ground-state $4f^6 6s^2$ configuration in Sm I were also measured [2,4]. J dependences of IS, resulting from the higher-order IS effect, i.e., the so-called crossed-second-order (CSO) effect or the far-configuration-mixing effect [5], were reported for the ground-state ^7F term of the $4f^6 6s^2$ configuration in Sm I [6,7]. However, these measurements of IS and hfs are all associated with the ground-state ^7F term and no measurement has been reported for J dependences of IS and hfs in the high-lying metastable states of the $4f^6 5d\,6s$ configuration. Particularly, there is no such study even for the lowest excited $4f^6 5d\,6s\ ^9H$ term, which has the same even parity as the ground-state ^7F term.

Therefore, it is most desirable to carry out measurements of hfs and IS associated with the high-lying metastable states of the $4f^6 5d\,6s$ configuration in Sm I. The CSO parameter z_{5d} for the $5d$ electron can be derived from such measurement and is useful to investigate the systematic behavior of z_{5d} for the rare-earth elements. A systematic behavior has been recently reported for the CSO parameters z_{4f} of the rare-earth elements and also z_{5d} of the $5d$ elements ($Z=71-79$), and it is interesting to find that the CSO effect is proportional to the degree of freedom of electrons (or holes) in the configuration [8]. In this paper we report the measurements of IS and hfs for the metastable states of the $4f^6 5d\,6s\ ^9H$ term in Sm I and discuss the J dependence in detail.

II. EXPERIMENT

Atomic-beam laser spectroscopy was used in this experiment. An atomic beam of Sm stable isotopes was produced using resistance heating of a molybdenum oven with a small orifice 0.5 mm in diameter and collimated with another office 2 mm in diameter. The collimation ratio was about 80 for the atomic beam. An electric discharge was used to populate the metastable states. A discharge cathode (helical coil 3 mm in diameter and 4 mm in length) made of a 0.5-mm-diam Ta wire was heated by a current of about 7 A. It was placed near the oven orifice along the beam direction. The oven temperature was monitored with a Pt-Rh thermocouple and controlled to be about 790 °C to obtain a Sm vapor pressure of 0.04 Torr. A large population in the metastable states was obtained with a discharge voltage of about 30 V and a current of about 400 mA.

An Ar-ion laser (Spectra-physics 2016) was used to pump a ring dye laser (Spectra-physics 380A) with rhodamine 6G dye. The laser beam was collimated by four slits and crossed perpendicularly the atomic beam. The fluorescent light from the atomic beam was focused by a spherical mirror and recorded by a cooled photomultiplier. For the relative frequency calibration, the laser light transmitted through a confocal Fabry-Pérot interferometer (FPI) with a free spectral range of 297.7 MHz was measured simultaneously with the fluorescence from the atomic beam. An $^{127}I_2$ cell was used to determine the absolute frequency of the transition. Details of the exper-

*Present address: Primo Co. Ltd., Mitaka, Tokyo 181, Japan.

imental setup have been already described elsewhere [9–11].

III. EXPERIMENTAL RESULTS

Isotope shifts and hyperfine structures of 12 transitions from the metastable ^9H_J ($J=1-7$) states of the $4f^6 5d6s$ configuration in Sm I were measured. The transitions and associated energy-level scheme [12] are shown in Fig. 1, and details about the lower and upper levels are summarized in Table I. To obtain J dependences of IS in the ^9H term, we chose the 12 transitions as seen in the figure, that is, measuring pairwise two different states of the ^9H term to the same upper state.

To examine the population in the metastable ^9H_J states, a transition of 582.26 nm from the first excited $^7F_1$ state of the ground-state $4f^6 6s^2$ configuration to the $4f^6 6s6p\ ^5G_2$ state was also measured, and is included in Fig. 1 and Table I. The fluorescence intensities of the 582.26-nm transition and 573.50-nm transition from the metastable $^9H_1$ state were measured at different discharge current and voltage. Then, all fluorescence peaks in each spectrum were integrated to obtain the dependences of the relative population on the discharge current and voltage. The results of the relative population for the first excited $^7F_1$ state and metastable $^9H_1$ state are shown in Fig. 2. The relative population was normalized at discharge current $I_D=0$ mA in (a) and discharge voltage $V_D=0$ V in (b) for $^7F_1$, and $I_D=600$ mA in (a) and $V_D=50$ V in (b) for $^9H_1$, respectively. It is seen from Fig. 2(a) that the relative population of the first excited $^7F_1$ state decreases with increase of I_D and that of the metastable $^9H_1$ state increases. This is reasonable because atoms in the thermally populated $^7F_1$ state are excited up to the metastable ^9H_J states by the electric discharge. Similar tendency is found in Fig. 2(b) for the dependence on V_D. The population of the metastable $^9H_1$ state reaches saturation at the discharge current of about 400 mA and voltage of about 30 V.

A typical fluorescence spectrum measured for the 588.83-nm transition is shown in Fig. 3. The even-mass

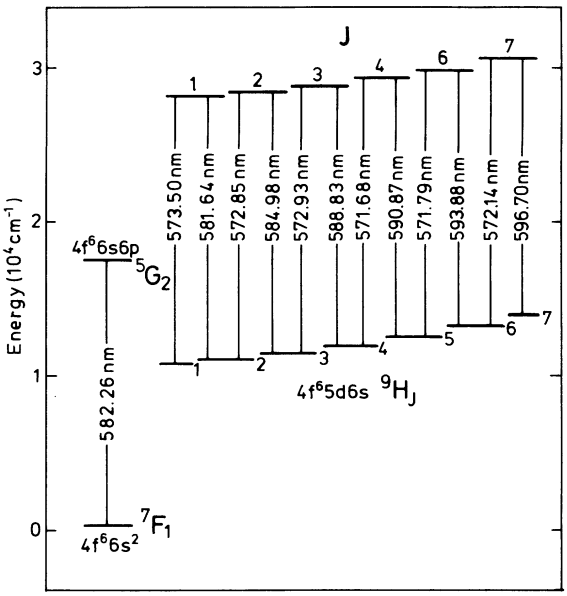

FIG. 1. Measured transitions and related energy-level scheme in Sm I.

isotopes ^{144}Sm, ^{148}Sm, ^{150}Sm, ^{152}Sm, and ^{154}Sm have no hfs and each isotope has only one peak. The odd-mass isotopes ^{147}Sm and ^{149}Sm, both with the nuclear spin $I=\frac{7}{2}$, have a rather narrow and complicated hfs compared with, for example, the 582.26-nm $^7F_1$-$^5G_2$ transition. The full width at half maximum (FWHM) of the peak is about 20 MHz and is mainly due to the Doppler broadening of the atomic beam and natural width of the upper level of the transition. The background in the spectrum is mainly due to the stray light of electric discharge scattered from the atomic beam. Many baffles were set along the atomic-beam path and the inside of the apparatus walls were painted black. Therefore, the radiation background from the oven and the stray light scattered from the apparatus walls were almost completely suppressed. Peak centers were determined from the least-squares fit with a Lorentz function and relative fre-

TABLE I. Wavelengths and energies of the studied transitions, and properties of the lower and upper states.

Wavelength	Transition energy	Lower state			Upper state		
(nm)	(cm^{-1})	Configuration	State	Energy (cm^{-1})	Configuration	State	Energy (cm^{-1})
582.26	17 169.79	$4f^6 6s^2$	$^7F_1$	292.58	$4f^6 6s6p$	$^5G_2$	17 462.37
573.50	17 431.98	$4f^6 5d6s$	$^9H_1$	10 801.10		$J=1$	28 233.08
581.64	17 188.18	$4f^6 5d6s$	$^9H_2$	11 044.90		$J=1$	28 233.08
572.85	17 451.67	$4f^6 5d6s$	$^9H_2$	11 044.90		$J=2$	28 496.57
584.98	17 090.07	$4f^6 5d6s$	$^9H_3$	11 406.50		$J=2$	28 496.57
572.93	17 449.26	$4f^6 5d6s$	$^9H_3$	11 406.50		$J=3$	28 855.76
588.83	16 978.26	$4f^6 5d6s$	$^9H_4$	11 877.50		$J=3$	28 855.76
571.68	17 487.53	$4f^6 5d6s$	$^9H_4$	11 877.50	$4f^5 5d6s^2$	$^7D_4$	29 365.03
590.87	16 919.68	$4f^6 5d6s$	$^9H_5$	12 445.35	$4f^5 5d6s^2$	$^7D_4$	29 365.03
571.79	17 484.03	$4f^6 5d6s$	$^9H_5$	12 445.35		$J=6$	29 929.38
593.88	16 833.63	$4f^6 5d6s$	$^9H_6$	13 095.75		$J=6$	29 929.38
572.14	17 473.43	$4f^6 5d6s$	$^9H_6$	13 095.75		$J=7$	30 569.18
596.70	16 754.28	$4f^6 5d6s$	$^9H_7$	13 814.90		$J=7$	30 569.18

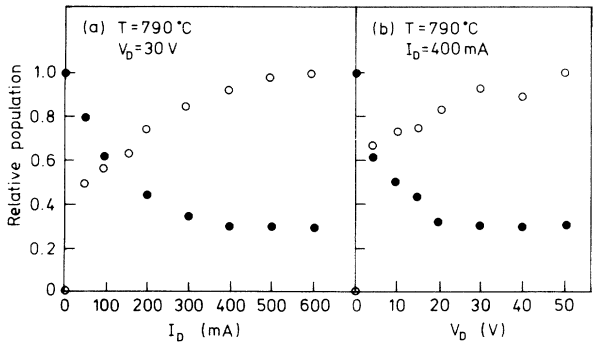

FIG. 2. Dependences of the relative population for the first excited $^7F_1$ state of the $4f^6 6s^2$ configuration (closed circle) and the metastable $^9H_1$ state of the $4f^6 5d 6s$ configuration (open circle) on the discharge current I_D (a) and discharge voltage V_D (b). The oven temperature and the discharge voltage (current) are fixed at $T=790$ °C and $V_D=30$ V for the case of (a), and $T=790$ °C and $I_D=400$ mA for the case of (b).

quencies between different peaks were determined by comparison with the FPI spectrum.

The hfs splittings and transitions of the odd-mass isotopes ^{147}Sm and ^{149}Sm are shown schematically in the upper part of Fig. 3. The hfs's of the metastable ^9H_J states and all of the upper states were not known except the $^9H_2$ and $^9H_3$ states [3]. The identification of the hfs peaks was done as follows. First, we measured the 581.64-nm $^9H_2$–upper $J=1$ transition and determined the hfs of the upper $J=1$ state. Second, from the measurement of the 573.50-nm $^9H_1$–upper $J=1$ transition, the hfs of the $^9H_1$ state was determined. In a similar way, from the measurement of the 572.93-nm $^9H_3$–upper

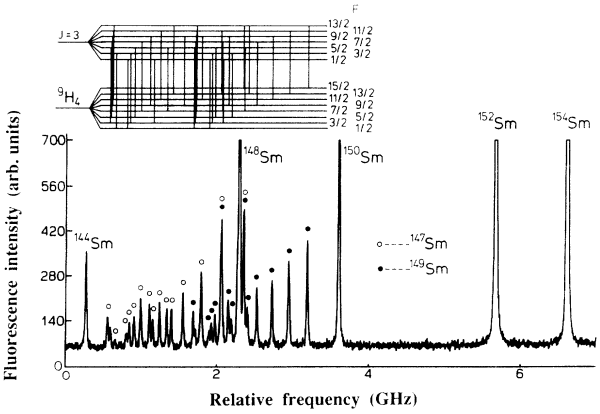

FIG. 3. Measured fluorescence spectrum of the 588.83-nm transition. The relative frequency scale of the horizontal axis was calibrated with the use of the FPI spectrum. Peaks of the even-mass isotopes are labeled with the isotopic symbols and the hfs peaks of ^{147}Sm and ^{149}Sm with the open and closed circles, respectively. The upper part in the figure shows the hfs splittings of the lower and upper levels of the 588.83-nm transition and also the transitions which correspond to the measured hfs peaks for ^{147}Sm and ^{149}Sm. F is the total angular momentum of the atom, that is, $F=I+J$.

$J=3$ transition, the hfs of the upper $J=3$ state was determined. Finally, from the 588.83-nm $^9H_4$–upper $J=3$ transition, the hfs of the $^9H_4$ state, and so on, was determined.

From the determined hfs splittings, the magnetic-dipole constants A and the electric-quadrupole constants B were obtained for ^{147}Sm and ^{149}Sm, and the isotope shifts for the odd-mass isotopes were deduced from the center of gravity. The hfs constants A and B for the metastable ^9H_J $(J=1-7)$ states of the $4f^6 5d 6s$ configuration in Sm I are presented in Table II. For the $^9H_2$ and $^9H_3$ states, the previous values A and B measured by Childs, Poulsen, and Goodman [3] by means of laser-rf double resonance are included in Table II for comparison. It is seen from Table II that there is reasonable agreement between the present work and previous measurements [3] and also some discrepancies outside the limits of error, e.g., the constant A of ^{149}Sm for $^9H_2$. Such discrepancy may be due to uncertainties, not included in the analysis, from the determination of peak centers in the case of double or triplet peaks; hfs spectra for ^{147}Sm and ^{149}Sm are so narrow that fluorescence peaks are always overlapped for the transitions studied. The hfs constants for the upper levels of the 12 transitions studied are also determined and are listed in Table III. The obtained isotope shifts of the stable isotopes are summarized in Table IV for the 12 transitions in Sm I.

IV. ANALYSIS AND DISCUSSION

A. J dependences of the hfs constants A and B for the ^9H term of the $4f^6 5d 6s$ configuration

From the hfs constants A and B, the single-electron hfs parameters $a_{nl}^{k_s k_l}$ and $B_{nl}^{k_s k_l}$ can be derived [13,14]. However, such an analysis is not possible for the present $4f^6 5d 6s$ configuration in Sm I because seven parameters of a_{4f}^{01}, a_{4f}^{12}, a_{4f}^{10}, a_{5d}^{01}, a_{5d}^{12}, a_{5d}^{10}, and a_{6s}^{10} and six parameters of b_{4f}^{02}, b_{4f}^{13}, b_{4f}^{11}, b_{5d}^{02}, b_{5d}^{13}, and b_{5d}^{11} should be considered for A and B, respectively. In the case of a pure LS-coupling state, the hfs constants A and B can be written as [9,15]

$$A=\alpha_{01}(J)R_{01}^{1}+\alpha_{12}(J)R_{12}^{1}+\alpha_{10}(J)R_{10}^{1}\ , \tag{1}$$

$$B=\beta_{02}(J)R_{02}^{2}+\beta_{13}(J)R_{13}^{2}+\beta_{11}(J)R_{11}^{2}\ , \tag{2}$$

where $R_{k_s k_l}^{K}$, being the linear combination of $a_{nl}^{k_s k_l}(b_{nl}^{k_s k_l})$ of the different electron shell nl, are the parameters to be determined. The coefficients $\alpha_{k_s k_l}$ and $\beta_{k_s k_l}$ are expressed as

$$\alpha_{k_s k_l}=\left[\frac{2J+1}{J(J+1)}\right]^{1/2}\begin{Bmatrix} S & S & k_s \\ L & L & k_l \\ J & J & 1 \end{Bmatrix}, \tag{3}$$

$$\beta_{k_s k_l}=\left[\frac{(2J+1)2J(2J-1)}{(2J+3)(2J+2)}\right]^{1/2}\begin{Bmatrix} S & S & k_s \\ L & L & k_l \\ J & J & 2 \end{Bmatrix}. \tag{4}$$

TABLE II. Measured hyperfine constants A and B (MHz) of ^{147}Sm and ^{149}Sm for the ^9H_J states of the $4f^6 5d\,6s$ configuration. The number in the parentheses after A or B indicates the mass number.

State	A(147)	A(149)	B(147)	B(149)
$^9H_1$	−78.25(21)	−61.85(19)	−3.01(76)	0.82(61)
$^9H_2$	−93.00(13)	−75.23(12)	−11.5(14)	3.17(14)
	−92.8699(4)[a]	−76.5683(4)[a]	−11.6586(20)[a]	3.2192(20)[a]
$^9H_3$	−122.32(14)	−100.70(15)	−20.2(20)	5.4(31)
	−122.1573(4)[a]	−100.6514(4)[a]	−20.8263(20)[a]	5.9040(20)[a]
$^9H_4$	−129.18(10)	−105.92(10)	−47.3(24)	13.4(19)
$^9H_5$	−147.17(18)	−124.66(19)	−86.0(55)	24.5(66)
$^9H_6$	−184.50(14)	−151.85(15)	−106.9(57)	32.2(63)
$^9H_7$	−219.49(16)	−184.75(13)	−126.6(82)	39.0(57)

[a]Reference [3].

TABLE III. Measured hyperfine constants A and B (MHz) of ^{147}Sm and ^{149}Sm for the high-lying upper levels.

Level (cm^{-1})	A(147)	A(149)	B(147)	B(149)
28233.08	−40.07(20)	−34.42(18)	26.37(69)	−11.95(58)
28496.57	−97.39(15)	−82.72(20)	−40.2(15)	11.5(24)
28855.76	−101.61(11)	−83.80(11)	−18.2(20)	5.1(21)
29365.03	−81.29(10)	−70.58(10)	−57.2(23)	16.7(23)
29929.38	−135.72(11)	−112.42(16)	−88.4(49)	27.7(49)
30569.18	−188.36(15)	−157.86(17)	−119.9(75)	39.5(78)

TABLE IV. Measured isotope shifts of stable isotopes for twelve transitions in Sm I.

Transition	Isotope shift (MHz)					
(nm)	154–152	154–150	154–149	154–148	154–147	154–144
573.50	−152.5(7)	−667.6(12)	−926.9(13)	−945.2(13)	−1086.2(17)	−1300.2(16)
581.64	−147.8(7)	−663.1(12)	−917.4(15)	−931.7(13)	−1061.5(20)	−1272.9(16)
572.85	−241.1(7)	−932.1(15)	−1279.4(16)	−1334.5(15)	−1532.6(16)	−1896.0(20)
584.98	−235.6(8)	−922.9(11)	−1259.6(18)	−1315.4(14)	−1507.8(16)	−1863.1(19)
572.93	−924.1(17)	−2967.2(27)	−3980.3(37)	−4294.0(41)	−4952.9(42)	−6387.5(52)
588.83	−909.8(9)	−2933.2(25)	−3935.1(31)	−4246.7(34)	−4895.9(38)	−6321.5(47)
571.68	−361.6(8)	−1309.2(16)	−1764.1(28)	−1876.1(19)	−2165.6(22)	−2707.3(24)
590.87	−338.3(11)	−1216.6(18)	−1634.4(19)	−1738.9(22)	−2001.7(24)	−2510.7(26)
571.79	−221.7(11)	−873.7(17)	−1203.8(19)	−1240.8(18)	−1421.0(19)	−1767.3(21)
593.88	−216.6(10)	−858.3(17)	−1178.9(21)	−1228.8(19)	−1401.7(19)	−1713.5(22)
572.14	−754.5(13)	−2480.5(18)	−3332.2(35)	−3580.4(34)	−4125.8(39)	−5296.8(44)
596.70	−743.6(10)	−2455.1(25)	−3293.3(34)	−3540.2(33)	−4079.0(40)	−5236.7(47)

TABLE V. Hyperfine parameters $R^1_{k_s k_l}$ and $R^2_{k_s k_l}$ (GHz) of ^{147}Sm and ^{149}Sm for the ^9H term of the $4f^6 5d\,6s$ configuration.

	R^1_{01}	R^1_{12}	R^1_{10}	R^2_{02}	R^2_{13}	R^2_{11}
^{147}Sm	−28.607(28)	23.990(43)	−12.041(10)	−6.69(72)	4.27(69)	−4.70(34)
^{149}Sm	−24.155(25)	20.688(39)	−9.959(9)	2.64(71)	−1.95(65)	1.60(35)

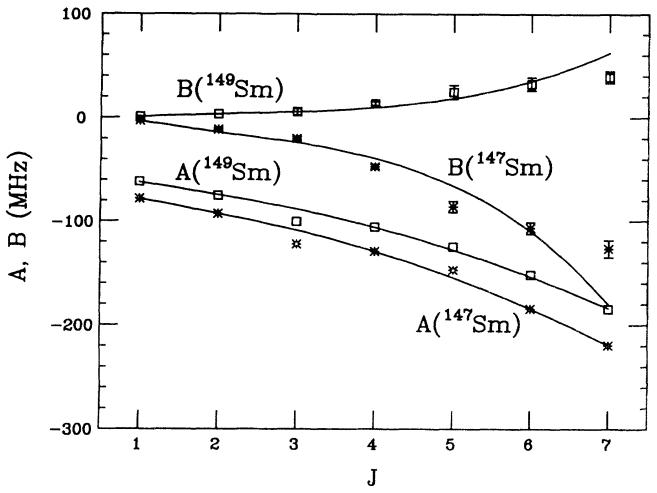

FIG. 4. J dependences of the hyperfine constants A and B of ^{147}Sm and ^{149}Sm for the ^9H term of the $4f^6 5d6s$ configuration. Lines show the results of the least-squares fits.

Since the intermediate-coupling wave function is not known, we assumed that the pure LS-coupling scheme for the ^9H_J state of the $4f^6 5d6s$ configuration in Sm I and the measured hfs constants A and B of ^{147}Sm and ^{149}Sm (Table II) for the ^9H_J ($J=1-7$) states were fitted using Eqs. (1) and (2). The obtained parameters $R^K_{k_s k_l}$ are listed in Table V for ^{147}Sm and ^{149}Sm. The fitted values A and B are shown in Fig. 4 together with the measured constants A and B. It is seen from Fig. 4 that the fitted values A and B are in good agreement with the measured values except at $J=3,5$ for A and $J=5,7$ for B, where large deviations are found. Such deviation should be attributed to the breakdown of the assumed pure LS coupling for these states. The hfs constants A of ^{147}Sm and ^{149}Sm show the same trend, while for B they have opposite trends as shown in Fig. 4. This is because ^{147}Sm and ^{149}Sm both have negative nuclear magnetic-dipole moments μ while the nuclear electric-quadrupole moments Q have opposite signs [16]. The hyperfine magnetic field A/μ and electric-field gradient B/Q produced at the nucleus by the electrons, however, have the same trends as they increase with increase of J, i.e., stronger hyperfine interactions for the ^9H_J state with larger J.

B. J dependences of the isotope shift for the ^9H term of the $4f^6 5d6s$ configuration

Since each of the two transitions among the measured 12 transitions are related to the same upper levels (see Fig. 1), the IS difference between the two transitions should be that between the lower ^9H_J states of the $4f^6 5d6s$ configuration, which is called the residual isotope shifts $T_{\rm res}$ [9]. Residual isotope shifts $T_{\rm res}$ were thus obtained for ^9H_J ($J=2-7$) with respect to $^9H_1$ of the $4f^6 5d6s$ configuration in Sm I, which are the measure of J dependences of IS within the ^9H term. Results of $T_{\rm res}$ for the different isotope pairs are listed in Table VI.

J dependences of IS derive from the crossed-second-order (CSO) effect [5]. The CSO effect between the magnetic interaction and IS operators leads to the J dependence of IS in a term of the pure configuration. The J dependence of IS is described by one parameter z_{nl} with the angular coefficient c_{nl}, which is the same one as the parameter in the spin-orbit interaction energy [5]. For the present $4f^6 5d6s$ configuration in Sm I, two parameters z_{4f} and z_{5d} should be taken into consideration. In the case of the pure LS-coupling scheme, the coefficients c_{4f} and c_{5d} have simply the same dependence on J, i.e., $\frac{1}{2}[J(J+1)-L(L+1)-S(S+1)]$. Thus, the residual isotope shift $T_{\rm res}$ can be written as

$$T_{\rm res}=\Delta c_{4f} z_{4f}+\Delta c_{5d} z_{5d} =\Delta c\left(\tfrac{3}{40} z_{4f}+\tfrac{1}{20} z_{5d}\right), \quad (5)$$

where $c=\frac{1}{2}[J(J+1)-L(L+1)-S(S+1)]$.

It was found that $T_{\rm res}$ at $J=5$ could not be expressed by Eq. (5) and this is in agreement with the results from the fits of A and B. It means that there is a strong deviation from LS coupling for the $^9H_5$ state. Thus, $T_{\rm res}$ at $J=5$ was not used in the following analysis. From $T_{\rm res}$ of Table VI, the CSO parameter z_{5d} was derived using the experimental parameter z_{4f} of the $4f^6 6s^2$ configuration in Sm I for the even-mass isotope pairs [17], assuming $z_{4f}(4f^6 5d6s)/z_{4f}(4f^6 6s^2)=\zeta_{4f}(4f^6 5d6s)/\zeta_{4f}(4f^6 6s^2)$ where the spin-orbit integral $\zeta_{4f}(4f^6 6s^2)$ is known [17], and assuming $\zeta_{4f}(4f^6 5d6s)$ to be equal to the known $\zeta_{4f}(4f^5 5d6s^2)$ [18] with an uncertainty of 10%. The obtained parameters z_{5d} are listed in Table VII for the even-mass isotope pairs.

TABLE VI. Residual isotope shifts $T_{\rm res}$ of the different isotope pairs for the ^9H_J states of the $4f^6 5d6s$ configuration in Sm I.

	$T_{\rm res}$ (MHz)					
State	154–152	154–150	154–149	154–148	154–147	154–144
$^9H_1$	0.0	0.0	0.0	0.0	0.0	0.0
$^9H_2$	5.0(10)	5.2(17)	10.4(20)	14.5(18)	25.9(26)	29.1(23)
$^9H_3$	11.0(15)	15.4(25)	31.5(31)	35.2(28)	52.6(35)	64.7(36)
$^9H_4$	26.0(24)	50.7(45)	78.3(57)	84.5(60)	111.9(66)	134.1(79)
$^9H_5$	50.1(28)	144.9(51)	210.1(67)	224.2(67)	278.6(74)	334.9(86)
$^9H_6$	56.1(31)	162.2(56)	237.4(72)	239.0(72)	301.2(79)	393.5(91)
$^9H_7$	68.0(35)	189.6(64)	278.8(87)	282.3(86)	351.6(96)	459(11)

TABLE VII. CSO parameters z_{5d} and z_{5d}/λ for the different isotope pairs in the ^9H term of the $4f^6 5d 6s$ configuration in Sm I.

Isotope pair	154–152	154–150	154–148	154–144	Average
z_{5d} (MHz)	37.8(33)	91(17)	142(19)	244(26)	
λ (fm^2)[a]	0.220(12)	0.624(25)	0.913(29)	1.407(39)	
z_{5d}/λ (MHz/fm^2)	172(18)	146(29)	155(21)	173(19)	165(10)

[a]Reference [20].

To investigate the contributions of the field shift and the specific mass shift in the CSO effect, we divide the values z_{5d} of the $4f^6 5d 6s$ configuration by the nuclear parameter λ [19,20], which is proportional to the field shift. The results are listed in Table VII. It is seen that the values z_{5d}/λ are constant for different isotope pairs within the uncertainties. This indicates that the field shift is the dominant contribution and the specific mass shift is negligible in the CSO effect. An average value of z_{5d}/λ is obtained to be 165(10) MHz/fm^2.

To compare the present z_{5d} value of Sm with the values of other elements, we use the normalized parameter $z_{5d\ \mathrm{norm}} = z_{5d}/(\lambda \zeta_{5d})$. Assuming ζ_{5d} of the $4f^6 5d 6s$ configuration to be equal to the known ζ_{5d} of the $4f^5 5d 6s^2$ configuration [18] with an uncertainty of 10%, we have $z_{5d\ \mathrm{norm}} = 7.9(13) \times 10^{-6}$ fm^{-2} for the $4f^6 5d 6s$ configuration in Sm I. This value is comparable with the values of $z_{5d\ \mathrm{norm}} = 6.29(60) \times 10^{-6}$ fm^{-2} for the $4f^7 5d 6s^2$ configuration in Gd I [9], $z_{5d\ \mathrm{norm}} = 6.3(17) \times 10^{-6}$ fm^{-2} for the $4f^7 5d 6s$ configuration in Gd II [21], and $z_{5d\ \mathrm{norm}} = 6.77(97) \times 10^{-6}$ fm^{-2} for the $4f^7 5d 6s$ configuration in Eu I [22]. To get further insight into the systematic behavior of $z_{5d\ \mathrm{norm}}$ for the rare-earth elements, more values z_{5d} of other elements are necessary.

ACKNOWLEDGMENT

This work was supported in part by the Sumitomo Foundation, Grant No. 92-103-672.

[1] W. J. Childs and L. S. Goodman, Phys. Rev. A **6**, 2011 (1972).
[2] H. Brand, B. Nottbeck, H. H. Schulz, and A. Steudel, J. Phys. B **11**, L99 (1978).
[3] W. J. Childs, O. Poulsen, and L. S. Goodman, Phys. Rev. A **19**, 160 (1979).
[4] H. Brand, B. Seibert, and A. Steudel, Z. Phys. A **296**, 281 (1980).
[5] J. Bauche and R.-J. Champeau, Adv. At. Mol. Phys. **12**, 39 (1976).
[6] R. New, J. A. R. Griffith, G. R. Isaak, and M. P. Ralls, J. Phys. B. **14**, L135 (1981).
[7] J. Bauche, R.-J. Champeau, and C. Sallot, J. Phys. B **10**, 2049 (1977).
[8] W. G. Jin, M. Wakasugi, T. T. Inamura, T. Murayama, T. Wakui, H. Katsuragawa, T. Ariga, T. Ishizuka, M. Koizumi, and I. Sugai, Phys. Rev. A **49**, 762 (1994).
[9] W. G. Jin, H. Sakata, M. Wakasugi, T. Horiguchi, and Y. Yoshizawa, Phys. Rev. A **42**, 1416 (1990).
[10] W. G. Jin, T. Horiguchi, M. Wakasugi, T. Hasegawa, and W. Yang, J. Phys. Soc. Jpn. **60**, 2896 (1991).
[11] W. G. Jin, T. Horiguchi, M. Wakasugi, T. Hasegawa, and W. Yang, Jpn. J. Appl. Phys. **30**, 1139 (1991).
[12] *Atomic Energy Levels, the Rare Earth Elements,* edited by W. C. Martin, R. Zalubas, and L. Hagan, Natl. Bur. Stand. Ref. Data Ser., Natl. Bur. Stand. (U.S.) Circ. No. 60 (U.S. GPO, Washington, DC, 1978).
[13] W. J. Childs, Phys. Rev. A **39**, 4956 (1989).
[14] V. Pfeufer, Z. Phys. D **4**, 351 (1987).
[15] P. G. H. Sandars and J. Beck, Proc. R. Soc. London Ser. A **289**, 97 (1965).
[16] P. Raghavan, At. Data Nucl. Data Tables **42**, 189 (1989).
[17] H.-D. Kronfeldt, D. Ashkenasi, and H. M. Nikseresht, Z. Phys. D **22**, 569 (1992).
[18] P. A. Carlier, J. Blaise, and M.-G. Schweighofer, J. Phys. (Paris) **29**, 729 (1968).
[19] E. W. Otten, in *Treatise on Heavy-Ion Science,* edited by D. A. Bromley (Plenum, New York, 1989), Vol. 8, p. 517.
[20] P. Aufmuth, K. Heilig, and A. Steudel, At. Data Nucl. Data Tables **37**, 455 (1987).
[21] J.-R. Kropp, H.-D. Kronfeldt, and R. Winkler, Z. Phys. A **321**, 57 (1985).
[22] P. Seifert, D.-J., Weber, H.-D. Kronfeldt, and R. Winkler, Z. Phys. D **14**, 99 (1989).